JMEPEG (2010) 19:751–760
DOI: 10.1007/s11665-009-9532-5

Damage Characterization and Real-Time Health Monitoring of Aerospace Materials Using Innovative NDE Tools

Theodore E. Matikas

(Submitted September 10, 2008; in revised form June 23, 2009)

The objective of this work is to characterize the damage and monitor in real-time aging structural components used in aerospace applications by means of advanced nondestructive evaluation techniques. Two novel experimental methodologies are used in this study, based on ultrasonic microscopy and nonlinear acoustics. It is demonstrated in this work that ultrasonic microscopy can be successfully utilized for local elastic property measurement, crack-size determination as well as for interfacial damage evaluation in high-temperature materials, such as metal matrix composites. Nonlinear acoustics enables real-time monitoring of material degradation in aerospace structures. When a sinusoidal ultrasonic wave of a given frequency and of sufficient amplitude is introduced into a nonharmonic solid, the fundamental wave distorts as it propagates, and therefore the second and higher harmonics of the fundamental frequency are generated. Measurements of the amplitude of these harmonics provide information on the coefficient of second- and higher-order terms of the stress–strain relation for a nonlinear solid. It is shown in this article that the material bulk nonlinear parameter for metallic alloy samples at different fatigue levels exhibits large changes compared to linear ultrasonic parameters, such as velocity and attenuation.

Keywords aerospace materials, elastic wave mechanics, interface characterization, nondestructive evaluation, nonlinear acoustics, structural health monitoring, ultrasonic microscopy

1. Introduction

Innovative nondestructive evaluation (NDE) methodologies based on linear and nonlinear acoustics are of utmost importance for developing damage tolerance approaches in aerospace materials by monitoring the accumulation of damage under cyclic loading.

High-strength titanium alloys, as well as fiber-reinforced metal matrix composite materials, are being considered for a number of applications because of their improved mechanical properties in high-temperature applications. In applications where cyclic loading is expected and where life management is required, consideration must be given to the behavior of the material in the vicinity of stress risers such as notches and holes. It is in these regions that damage initiation and accumulations are expected. In the case of metal matrix composites for aircraft structural and engine components, several damage modes near stress risers have been identified (Ref 1). One important damage mode under cyclic loading is the nucleation and growth of matrix cracks perpendicular to the fiber direction. In some composite systems, the matrix crack growth occurs without the corresponding failure of the fibers. This process results in the development of relatively large matrix cracks that are either fully or partially bridged by unbroken fibers. The presence of bridging fibers can significantly influence the fatigue crack growth behavior of the composite. To develop a life prediction methodology applicable to these composite systems, an understanding must be developed of both the matrix cracking behavior as well as the influence of the unbroken fibers on the crack driving force and the affect of interfacial degradation and damage on the eventual failure of the composite.

Paramount to understanding the influence of unbroken fibers is to identify the mechanisms which transfer the load from the matrix to the fiber. The mechanics of matrix cracking and fiber bridging in brittle matrix composites has been addressed (Ref 2, 3). The analysis is based on the shear lag model to describe the transfer of load from the fiber to the matrix. In the shear lag model, the transfer of load occurs through the frictional shear force (τ) between the fiber and the matrix. The analyses indicate that size of the region on the fiber over which τ acts can have a significant effect on the influence of unbroken fibers on crack growth rate behavior. However, although some indirect ultrasonic experimental techniques have been developed to determine the extent of influence of τ (Ref 4-6), no direct nondestructive experimental techniques currently exist. Another important interfacial phenomenon is the degradation, fracture, and/or failure of the interface resulting from crack initiation and growth, which is an aspect of interest in this article.

This work has an objective to demonstrate the utility and versatility of ultrasonic microscopy and nonlinear acoustics for material behavior research of aerospace materials. Ultrasonic

---

Theodore E. Matikas, Department of Materials Science and Engineering, University of Ioannina, University Campus, 45110 Ioannina, Greece. Contact e-mail: matikas@cc.uoi.gr.

microscopy has been developed to nondestructively determine regions of interfacial degradation while, simultaneously, providing indications of surface crack length in metal matrix composite samples subjected to various testing conditions, including isothermal mechanical and thermomechanical fatigue. Furthermore, the damage accumulated in titanium alloys has been monitored in situ while the material was undergoing mechanical fatigue. The new technique enabled to measure the nonlinearity parameter of the material in real time, during the fatigue test. Low cycle experiment on titanium samples with duplex microstructure show a large increase of nonlinearity due to the accumulation of damage in the material. A good correlation between the material nonlinearity and the dislocation density has been observed.

2. Ultrasonic Microscopy

Ultrasonic microscopy is a nondestructive technique based on scanning acoustic microscope which was developed by Quate et al. (Ref 7, 8) and has been extensively further developed by Briggs et al. (Ref 9-13). The principle of operation of ultrasonic microscopy is based on the production and propagation of surface acoustic waves (SAW) as a direct result of a combination of the high curvature of the focusing lens of the transducer and the defocus of the transducer into the sample (Ref 7, 14). The most important contrast phenomenon in this technique is the presence of Rayleigh waves which are leaking toward the transducer and are very sensitive to local mechanical properties of the materials being evaluated (Ref 15). The generation and propagation of a leaky Rayleigh wave is modulated by the material's properties, thereby making it feasible to image even very subtle changes of the mechanical properties. The sensitivity of the SAW signals to surface and subsurface features depends on the degree of defocus and has been documented in the literature as the $V(z)$ curves (Ref 16). A $V(z)$ curve is obtained when the transducer, kept over a single point, is moved toward the specimen. Then, the signal, rather than simply decreasing monotonically, can undergo a series of oscillations. The series of oscillations at a defocus distance can be associated with Rayleigh wave excitation and interaction of a SAW with the specular reflection received directly by the transducer. The Rayleigh wave velocity, v_R, can then be calculated using a simple relationship:

$$v_R = \frac{v_o}{\sqrt{1 - \frac{v_o}{2\omega \Delta z}}} \qquad \text{(Eq 1)}$$

where v_o is the sound velocity in the coupling medium, ω is the frequency of ultrasound, and Δz is the periodicity of the $V(z)$ curve.

The defocus distance also has another important effect on the SAW signal obtained by the SAM transducer and dictates whether the SAW signal is separated in time from the specular reflection or interferes with it. Thus, depending on the defocus, the technique can be used either to map the interference phenomenon in the first layer of subsurface fibers or to map the surface and subsurface features in the sample.

The conventional technique for measuring SAW velocity is based on a $V(z)$ curve acquisition and analysis procedure utilizing a tone-burst system to interrogate the sample at a specific frequency using specially designed acoustic lenses. This technique requires calibration of the transducer's lens and electronics using a $V(z)$ curve obtained from a sample made of lead, which is a material that does not exhibit SAW. This procedure requires specialized instrumentation, which is time consuming, and cannot be used for on-line measurements in interrupted testing mode.

The new ultrasonic microscopy method presented here overcomes the limitations of the conventional technique because it is based on automated SAW velocity determination via $V(z)$ curve measurements using short-pulse ultrasound. The configuration of such system is presented in Fig. 1. The sensor used is a highly focused ultrasonic transducer with a central frequency of 50 MHz. The method employed here is self-calibrated, and is used to obtain Rayleigh velocity maps of the specimen through automated $V(z)$ curve acquisition and analysis (Ref 17). The automated $V(z)$ curve process for the characterization of fiber-reinforced composites is summarized as follows:

(a) Ultrasonic data are collected using a pulsed ultrasonic system and a specially designed, highly focused ultrasonic transducer. The basic data consist of a series of

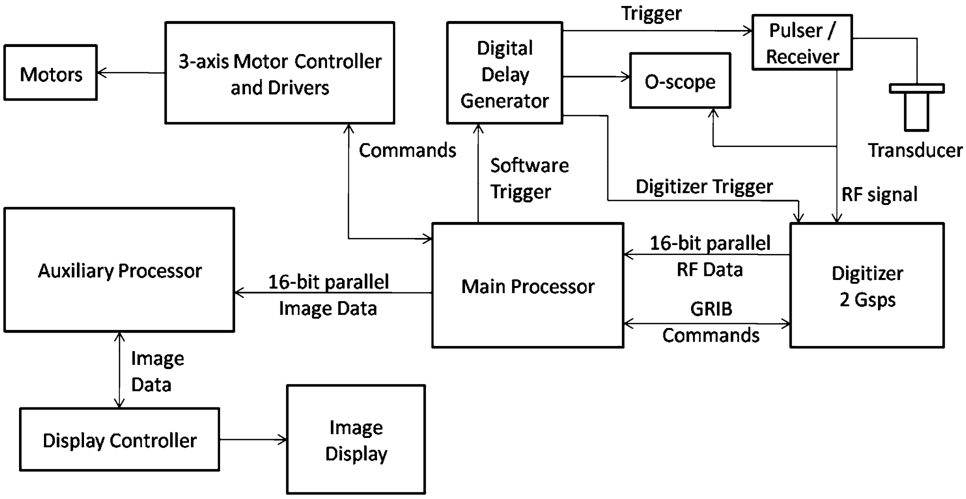

Fig. 1 Configuration of a short-pulse ultrasonic system for automated SAW velocity measurements

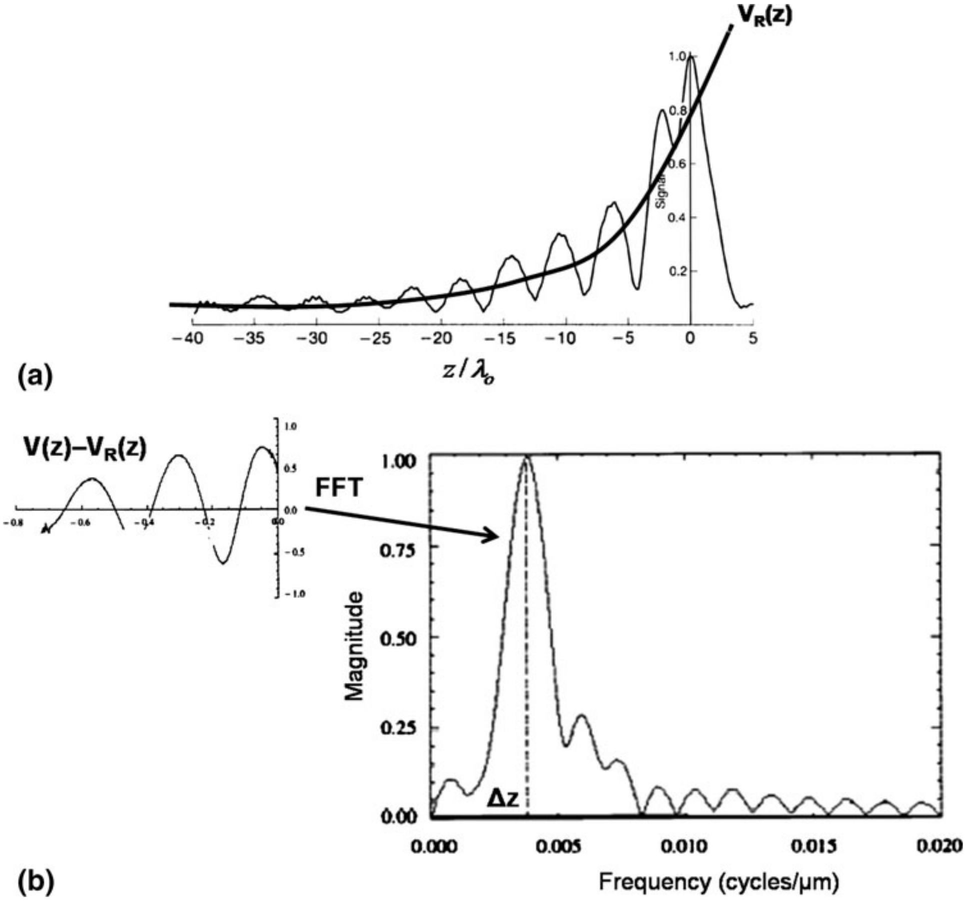

Fig. 2 The $V(z)$ curve method for determining Rayleigh velocity. (a) Self-calibrated reference curve $V_R(z)$. (b) Fast Fourier Transform of the $V(z)$–$V_R(z)$ curve

A-scans corresponding to various defocus distances. The waveforms are stored as two different B-scans: one containing the entire signal and the other containing a time-gated portion of the signal that corresponds to specular reflection.

(b) The magnitude of the time-gated signal in the Fourier domain is plotted for a selected ultrasonic frequency as a function of defocus distance. This provides a self-calibrated reference $V_R(z)$ curve (Fig. 2a).

(c) The magnitude of the entire A-scan in the Fourier domain is plotted for a specific frequency as a function of defocus distance. The calculated $V(z)$ curve and the reference $V_R(z)$ curve are then processed to compute the Rayleigh velocity of the material at the point where the data are collected (Fig. 2b).

The resolution of the technique for characterizing individual fibers and determining interfacial properties strongly depends on the lens defocus from the surface of the sample. In addition, it should be underlined that the choice of the coupling medium is essential for resolving individual fibers in the composite, since, for a specific ultrasonic transducer with a fixed lens curvature, the generation of Rayleigh waves on the surface of the composite only depends on the sound velocities of the coupling medium and of the material under interrogation. Based on Snell's law, the curvature of a transducer's lens required to generate SAW in a material is given by the relationship:

$$\theta = \sin^{-1}\left(\frac{c_{\text{coupling}}}{c_{\text{material}}}\right) \qquad \text{(Eq 2)}$$

where θ is the half-arc of the lens, and c_{coupling} and c_{material} are the ultrasonic velocities of the coupling medium and the material, respectively.

Figure 3 shows ultrasonic microscopy imaging of a Ti-24Al-11Nb/SCS-6 composite subjected to thermomechanical fatigue (TMF) using a highly focused 50 MHz transducer, designed to generate SAW in metals such as titanium and steel with water as a coupling medium. Due to environmental exposure, oxides were formed on the material's surface. This altered the sound velocity of the surface of the composite and, therefore, SAW could not be generated (Fig. 3a). The use of methanol as a coupling medium alleviated this difficulty (Fig. 3b).

The capability of ultrasonic microscopy to determine cracks size and evaluate interfacial damage is depicted in Fig. 4. This figure shows the first ply of a TiMetal21S/SCS-6 unidirectional composite with a circular hole, which underwent isothermal mechanical fatigue for 10^5 cycles at a frequency of 1 Hz and maximum applied stress of 600 MPa. The loading direction is in the direction of SCS-6 fibers. Several matrix cracks are clearly observed in Fig. 4. Crack bridging by unbroken fibers

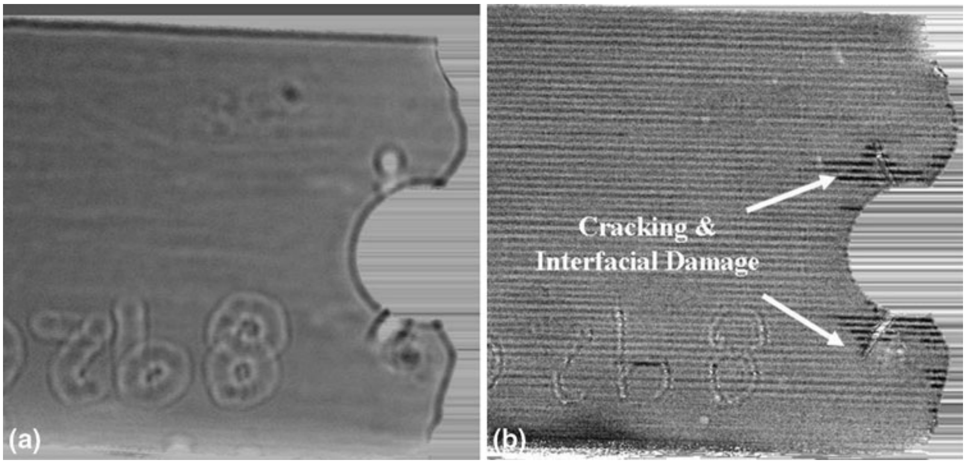

Fig. 3 The role of coupling medium in ultrasonic microscopy of metal matrix composites (Ti-24Al-11Nb/SCS-6 composite system subjected to TMF). (a) Use of water as the coupling medium. (b) Use of methanol as the coupling medium

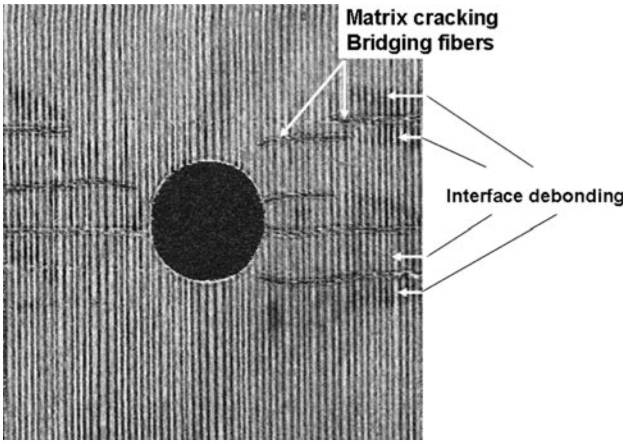

Fig. 4 Ultrasonic microscopy images at 50 MHz of a TiMetal21S/SCS-6 unidirectional composite with a circular hole, which underwent isothermal fatigue

resulting to interface debonding was found to dominate the fatigue crack growth life as evidenced by the characteristic decrease in crack growth rates as the crack length increased during fatigue cycling.

3. Real-Time Nonlinear Acoustics

The results presented in this section focus on the development of an innovative NDE nonlinear acoustics technique, which is sensitive to early stages of the fatigue process. This is essential to enhance the understanding and predict fatigue failure in critical components used in aerospace applications. Failures of engine components, which often occur much earlier than predictions by initial design, increase the need for reliable NDE methods for early fatigue damage characterization. In this study, a ($\alpha + \beta$) titanium alloy (Ti-6Al-4V) with duplex and beta annealed microstructure has been examined to validate the nonlinear acoustics technique. This microstructure has a good combination of crack initiation and crack propagation resistance. The material tested is similar to the material used in aircraft engine fan blades (Ref 18).

To characterize fatigue mechanisms using acoustic waves, it is necessary to understand the physics of propagation of acoustic or elastic waves in solids and also the physics involved in the process of fatigue damage in materials. In this direction, Granato and Lucke theory (Ref 19), known as the "vibrating string model of dislocation damping" developed in the 1950s, is the starting point for all the theories on acoustic wave interaction with dislocations.

It is well known that linearized relation between stress and strain "linearized Hooke's law" is sufficient to describe the mechanical properties of solids. The Hooke's law provides a way to relate stress to strain through the second-order elastic constants or moduli of the solid. The linear approximation allows the properties of the material that can be measured experimentally to two properties, namely, the velocity of sound (elastic modulus) and attenuation (damping) in the material. However, it has been shown (Ref 20) that these parameters are not robust enough to describe the fatigue mechanism. Generally, a solid possesses nonlinear elastic behavior, but for practical engineering applications and for the purpose of simplification it is ignored and treated as a linear material. Thus, it is necessary to understand acoustic wave propagation in nonlinear elastic material. Introduction of nonlinear terms into stress–strain relationship leads to inclusion of higher-order elastic constants.

A thermodynamic definition of nth-order elastic constant for the adiabatic constant is given by

$$C^{S}_{ijkl\ldots} = \rho_0 \left(\partial^n U \big/ \partial \eta_{ij} \partial \eta_{kl\ldots} \right)_S \qquad \text{(Eq 3)}$$

and the isothermal constant by

$$C^{T}_{ijkl\ldots} = \rho_0 \left(\partial^n F \big/ \partial \eta_{ij} \partial \eta_{kl\ldots} \right)_T \qquad \text{(Eq 4)}$$

where ρ_0 denotes density, U the internal energy, F the free energy, S the entropy, and T the temperature. Since the difference between adiabatic and isothermal constants is usually small, it is often ignored in experiments.

The wavelength of the sound waves in materials used in harmonic generation experiments is quite large compared with the interatomic spacing, typically, six orders of magnitude greater than the interatomic spacing. The number of atoms affected by one period of vibration, then, is of the order of 10^6, so the solid can be regarded as an elastic continuum, and the theory of finite deformations in the Lagrangian formulation can be applied. When considering the equation of motion of an elastic wave propagating through a solid, the latter is considered to be a lossless and perfectly elastic continuum.

A pure longitudinal wave propagating in a solid generates its own second harmonic. The differential equation of motion can be expressed in a form, in which the linear and nonlinear terms are separated:

$$\rho_0 \ddot{u} = \alpha \frac{\partial^2 u}{\partial a_i^2} + \delta \frac{\partial u}{\partial a_i}\left(\frac{\partial^2 u}{\partial a_i^2}\right) \qquad \text{(Eq 5)}$$

where α and δ give the expressions of elastic constants for each direction. It should be noted that the coefficient α is expressed in terms of second-order elastic constants only, but δ is expressed in terms of both second- and third-order elastic constants. By applying a perturbation solution to Eq 5 of the form:

$$u = u^0 + u' \qquad \text{(Eq 6)}$$

where $u' \ll u^0$, and use trial solution:

$$u^0 = A\sin(ka - \omega t) \quad \text{for} \quad \delta = 0 \qquad \text{(Eq 7)}$$

and

$$u' = Ba\sin[2(ka - \omega t)] + Ca\cos[2(ka - \omega t)] \qquad \text{(Eq 8)}$$

Substituting Eq 6 into Eq 5, one obtains:

$$\rho_0 \ddot{u}^0 = \rho_0 \ddot{u}' - \alpha \frac{\partial^2 u^0}{\partial a^2} - \alpha \frac{\partial^2 u'}{\partial a^2} = \delta \frac{\partial (u^0 + u')}{\partial a} \frac{\partial^2 (u^0 + u')}{\partial a^2} \qquad \text{(Eq 9)}$$

From the linear elastic equation of motion, the following relation is given:

$$\rho_0 \ddot{u}^0 - \alpha \frac{\partial^2 u^0}{\partial u^2} = 0 \qquad \text{(Eq 10)}$$

where the phase velocity $C_0 = (\alpha/\rho_0)^{1/2}$. Therefore, Eq 9 reduces to

$$\rho_0 \ddot{u}' - \alpha \frac{\partial^2 u'}{\partial a^2} = \delta \left[\frac{\partial u^0}{\partial a} \frac{\partial^2 u^0}{\partial a^2} + \left(\frac{\partial u'}{\partial a} \frac{\partial^2 u^0}{\partial a^2} + \frac{\partial u^0}{\partial a} \frac{\partial^2 u'}{\partial a^2} \right) + \frac{\partial u'}{\partial a} \frac{\partial^2 u'}{\partial a^2} \right] \qquad \text{(Eq 11)}$$

Since $u' \ll u^0$, the second and third terms on the right-hand side of Eq 11 can be neglected in comparison with the first. Therefore, to a first approximation the equation reduces to

$$\rho_0 \ddot{u}' - \alpha \frac{\partial^2 u'}{\partial a^2} = \delta \left(\frac{\partial u^0}{\partial a} \frac{\partial^2 u^0}{\partial a^2} \right) \qquad \text{(Eq 12)}$$

The approximated solution of this equation involving the second harmonic is given by

$$u(a,t) = A\sin(ka - \omega t) - \frac{a\delta k^2 A^2}{8\rho_0 C_0^2}\cos[2(ka - \omega t)] \qquad \text{(Eq 13)}$$

where $\alpha = \rho_0 C_0^2$, ω is the angular frequency, k is the wavenumber, and $C_0 = \omega/k$ is the phase velocity.

The ultrasonic nonlinearity parameter β is then defined as the negative ratio of the nonlinear term to the linear term in the wave equation. Equation 13 can be rewritten as follows:

$$u(a,t) = A\sin(ka - \omega t) + \frac{a\beta(kA)^2}{8}\cos[2(ka - \omega t)] \qquad \text{(Eq 14)}$$

The amplitude A of the first term and $a\beta(kA)^2/8$ in the second term in Eq 14 are, respectively, the fundamental amplitude A_1 and the second harmonic amplitude A_2. Therefore, the nonlinearity parameter, β, can be expressed in terms of the amplitudes A_1 and A_2:

$$\beta = \frac{8}{ak^2}\left(\frac{A_2}{A_1^2}\right) \qquad \text{(Eq 15)}$$

where a is the propagation distance and $k = 2\pi/\lambda$ is the propagation constant. When the attenuation of the fundamental wave α_1 and that of the second harmonic α_2 are taken into account, Eq 15 becomes:

$$\beta = \frac{8}{k^2}\left(\frac{A_2}{A_1^2}\right) \cdot \left[\frac{\alpha_2 - 2\alpha_1}{1 - e^{-a(\alpha_2 - 2\alpha_1)}}\right] \qquad \text{(Eq 16)}$$

In the measurement of nonlinearity parameter under cyclic loading, the change in β is more important than its absolute values. Hence, measurements of relative changes in the nonlinearity of the material from the virgin state to a fatigued state are examined in this work. Therefore, the β parameter defined in Eq 15 normalized by the value β_o (nonlinear parameter of the material at the virgin state) is experimentally measured.

The piezoelectric detection of second harmonic ultrasonic amplitude is based on propagating a pure single frequency f signal through the sample. As the elastic signal propagates through the medium, it is distorted as the result of the anharmonicity of the crystalline lattice and other microstructural disturbance, such as the grain boundaries and dislocations. During the fatigue process of Ti-6Al-4V, the lattice anharmonicity remains constant since the stress level applied to the specimen is far below the yield strength, i.e., in the elastic region. However, the other factors like grain boundaries, dislocations, and other impurities change as a function of fatigue level. The distorted signal is composed of the combination of the harmonics and grows as it propagates until the attenuation factor stops its growth. The harmonic portion of the distorted ultrasonic signal is very sensitive to the changes in the strain energy density due to the changes of these factors. In this work, the second harmonic signal, of frequency $2f$, is detected at the other end of the specimen by a second piezoelectric transducer and using a bandpass filter with a rejection ratio better than 60 dB. The transducer was manufactured using 36° Y-cut $LiNbO_3$ crystals placed inside specially designed brass housing and Plexiglas tubing. Lithium niobate single crystals were used since they are linear materials and also exhibit higher electromechanical coupling compared to quartz crystals.

New transducer holder and the grips for the fatigue load frame were designed to enable on-line monitoring of the material's nonlinearity parameter during the fatigue process, since the conventional grips are inadequate for attaching transducers to the specimen.

The experimental configuration for on-line piezoelectric detection of second harmonic signal during mechanical fatigue is based on a tone-burst generator and a power amplifier to launch longitudinal sound waves into the specimen at a frequency of 10 MHz. A high-power bandpass filter was placed between the power amplifier and the transducer to make sure that unwanted harmonic signals are filtered out. The same transducer was used to detect the fundamental signal reflected from the other end of the specimen. A 20 MHz transducer bonded to the other end of the specimen was used to receive the second harmonic signal. After the second harmonic signal is detected, it was fed to a linear narrow band amplifier through a 20 MHz bandpass filter. Both fundamental V_1 (mV) and second harmonic V_2 (mV) signals were sent to the D/A converter for digitization and the nonlinearity parameter was finally determined from the sampled signals.

Since it measured the nonlinear property of the specimen, it was necessary to verify that the measurement setup itself was linear indeed. For checking the system's linearity, a simple experiment was performed with an unfatigued Ti-6Al-4V sample at room temperature by changing the input voltage to the transmitting transducer. It was thus demonstrated that the slope of the curve of the amplitude of second harmonic versus the fundamental was linear. Since the measurement requires a relatively long time for a fatigue frequency of 1 Hz, it is necessary to check the stability of the system over a period time. The amplitudes of the fundamental and second harmonic signals were monitored over a period of 24 h in the laboratory and only small, almost negligible compared to the size of the measured values, fluctuations were observed during the fatigue test.

The experimental technique described above was used to measure the nonlinear acoustic properties of Ti-6Al-4V alloys and characterize on-line their fatigue behavior. Titanium alloys are widely used in aerospace applications because of their low density and high strength, good corrosion resistance, and good mechanical properties at elevated temperature (up to 600 °C). Titanium alloys are classified as α, ($\alpha + \beta$), or β according to the amount of α-stabilizing elements, such as aluminum, and of β-stabilizing elements, such as molybdenum, vanadium, chromium, niobium, iron, and manganese. Ti-6Al-4V is an important titanium alloy which is used in a wide variety of aerospace components. With a strength-to-density ratio of 25×10^6 mm, Ti-6Al-4V is an effective lightweight structural material and has strength-toughness combinations between those of steel and aluminum alloys. At room temperature, Ti-6Al-4V alloy is about 90 vol.% α, thus α phase dominates the physical and mechanical properties of this alloy. However, the overall effects of processing history and heat treatment on microstructure are complex. The microstructure depends on both processing history and heat treatment, and the microstructure that combines highest strength and ductility is not necessarily the microstructure that provides optimum fracture toughness or resistance to crack growth. The fatigue properties of the two-phase $\alpha + \beta$ alloys are strongly affected by the morphology and arrangement of both α and β phases. Basically, fully lamellar (β-annealed microstructure), fully equiaxed, and duplex (primary, α phase in a lamellar matrix) microstructure can be developed in $\alpha + \beta$ alloys. Fatigue cracks in fully lamellar microstructures nucleate at slip bands within the alpha lamellae or at alpha zones prior beta grain boundaries. Because both resistance to dislocation motion and resistance to fatigue crack nucleation depend on the width of the alpha lamellae, there is a direct correlation between fatigue strength and yield stress.

During the fatigue tests, the samples were subjected to cyclic loading at the frequency of 1 Hz under low cycle fatigue (LCF) conditions ($\sigma_{\max} = 850$ MPa, and R ratio = 0.1). The ultrasonic velocity and nonlinear property were measured at zero load on the sample, at an interval of 100 cycles of fatigue.

Attenuation and velocity of longitudinal sound wave measurements were performed at a frequency of 10 MHz at various stages of fatigue. It was observed that the longitudinal velocity of sound had a measurable change in the beginning of the fatigue process. As the fatigue process continues, there was an indication of reduction in the sound velocity beyond the 20% of the fatigue lifetime. During the processes of fatigue there may be small increase in the specimen length. For an accurate determination of the velocity of sound, it is necessary to incorporate the changes in the specimen length. Since length changes were not monitored during fatigue, no attempt has been made to correct the sound velocity changes.

Additionally, it was observed that the attenuation increased significantly in the initial stages of fatigue. It was further increased up to about 50% until the fatigue life reached 20% of the entire lifetime, and then remained fairly constant up to 40% of lifetime. The initial increase of 50% is quite significant; however, it is less sensitive to fatigue process beyond 20% of the fatigue life. The higher attenuation at the higher fatigue cycles may indicate an increase in the scattering of sound waves due to the increased dislocation dipole density from fatigue. As the increase in dislocation density saturates, the level of scattering of sound wave within the material becomes stable. It should be pointed out, however, that the general tendency of dislocation movement is known to migrate to the surface of the material. This could mean that the attenuation measurement in the bulk is less meaningful throughout the entire lifetime of the material.

Variation in amplitude of the second harmonic signal, as the amplitude of the fundamental signal is changed, is used for measurement of nonlinear acoustic behavior of the material. As the material is fatigued, the amplitude of the second harmonic signal increases to give a steeper slope.

Figure 5 shows the dislocation density and material nonlinearity as a function of the number of cycles. It can be observed in Fig. 5 that acoustic nonlinearity of the material exhibits large changes during the fatigue process. This finding is in contrast with the measurements of attenuation and elastic behavior, where the majority of variation occurred before the 20% of fatigue lifetime. The second harmonic signal generated during the fatigue process is not only sensitive to the early stage of the process but also to later stages of damage. This implies that the harmonic signal is very sensitive to the microstructural changes in the material. The variation of nonlinearity continues due to the generation of additional dislocation dipoles by the fatigue process and their interaction with the acoustic waves, as predicted by relevant models and experimental work (Ref 20-22).

Observing the variation of material nonlinearity as a function of fatigue damage in Fig. 5, the following conclusions can be drawn:

(a) The nonlinearity parameter remains almost constant (30% increase) during the first 10 to 20% of the life (Region I of the curve). Also during this period, the parameter is unstable.

(b) After this first region, the parameter increases linearly for about 40 to 50% of fatigue life cycles (Region II). At the end of this period, the total increase of the material nonlinearity from the virgin state is about 100%.

(c) At about 50 to 60% of fatigue life and up to final fracture of the specimen, the parameter exhibits a plateau (Region III).

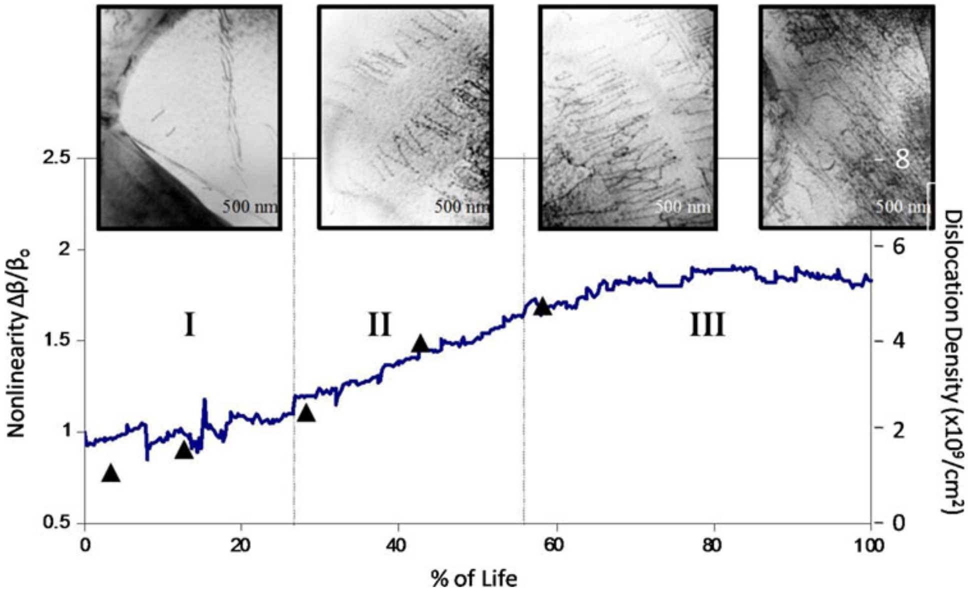

Fig. 5 Normalized nonlinearity (line plot) of Ti-6Al-4V samples as a function of fatigue level and correlation with transmission electron microscopy analysis of dislocation density (data points)

The above observations were made for all specimens investigated and can be considered as nonlinear acoustic ''signature'' behavior for the Ti-6Al-4V material. This behavior was correlated with transmission electron microscopy (TEM) to understand its mechanism in terms of changes in microstructure. Dog bone samples of the same microstructure obtained from other plates were used to fatigue the samples under similar fatigue conditions. Each sample was fatigued to a particular stage and a thin slice of the central section was taken for TEM measurements. TEM samples were prepared from the fatigue specimens in a very controlled, precise manner so that no new deformation is introduced into the material. First, the 2 mm section of the fatigue specimens was ground with 400 grit paper to a thickness of 125 to 150 µm. Next, a 3 mm diameter disk was core drilled from the section. The disk was then dimpled so that the thickness of the region in its center was reduced down to 25 µm. Finally, to avoid changing the dislocation density, thinning was carefully performed at the center of the disk by ion milling with a 4 kV Ar + beam and a 12° incidence angle, forming a small perforation until electron transparency is obtained. Around this perforation, the transmission electron microscopy was conducted. The TEM imaging was performed at a magnification of 60,000×.

Figure 5 shows TEM images obtained on samples at different levels of fatigue, along with the plot of continuous changes in nonlinear acoustic parameter normalized to the virgin state. The TEM analysis of the dislocation density in Fig. 5 shows least amount of damage during Region I of 10% fatigue while the acoustic nonlinearity remains almost the same as in the virgin material. In Region II, where the nonlinearity begins to increase, the TEM analysis shows development of dislocations in the lamellar zone. In Region III, where the nonlinearity begins to saturate, the TEM analysis shows significant increase in dislocation density and the microstructure seems to show formation of cellular regions inside the grains. The final TEM analysis shows increased dislocation density, fully developed cellular regions, and a completely messed up microstructure. Here, the nonlinearity has reached saturation and do not exhibit further increase (plateau).

A quantitative analysis of the TEM images was performed to determine the dislocation density. The projected length of dislocation lines, l_p, in the TEM images was measured using image analysis software. Assuming that the dislocations are randomly oriented, l_p, can be related to the length of dislocation lines, l (Ref 23):

$$l = \frac{4}{\pi} l_p \qquad \text{(Eq 17)}$$

The dislocation density is than given by

$$\rho = \frac{l}{V} = \frac{l}{At} \qquad \text{(Eq 18)}$$

where V is the volume of the observed material, A is the corresponding area, and t is the sample thickness, estimated by application of a graphical method (Ref 24) to convergent beam electron diffraction data (Ref 25).

A plot of the variation of dislocation density is shown in Fig. 5, together with the plot of the continuous change in nonlinear acoustic parameter, normalized to the specimen's virgin state. The dislocation density has been measured only up to 40% of fatigue life due to the fact that when the dislocation density becomes very large it is quite difficult to quantitatively determine its value using TEM. It is clear that the nonlinearity increases as the dislocation density increases and follow closely up to a fatigue life of about 30%. Beyond this, as the dislocation density increases, the nonlinearity does not follow the same curve. There are several reasons for this difference. Nonlinearity is measured over the entire volume of the material and as the fatigue cycles increase, the region of dislocation density is observed only in the central region of the sample. Hence, nonlinearity measurements are average over undamaged, less damaged, and heavily damaged regions. On the other hand, in TEM measurements, the dislocation density is estimated only from the central region of the sample and it will observe only maximum damaged region. A fair comparison should be with average density measured over the entire region of the sample. Second factor for this difference is that the nonlinearity is not only dependent on the dislocation density but also on the network structure. As the dislocation density increases, network formation also increases. It is necessary to include the contribution from different network formations for comparison. Such estimation has not been performed in TEM analysis at present.

In addition to on-line measurements of material nonlinearity parameter, localized measurements were performed on slices of samples fractured in a fatigue test at discreet positions along their length all the way from the fractured edge into the grip section. The nonlinearity parameter was compared with TEM images obtained almost in the same regions of samples that were fatigue-fractured under similar, LCF and high cycle fatigue (HCF), conditions and having similar fatigue life. Variation in dislocation density determined using TEM images at the same location are compared with the acoustic nonlinear parameter.

Figure 6(a) shows the variation of absolute values of nonlinearity parameter for samples fatigue-fractured under LCF conditions, and measured at eight different locations between the fractured edge and the grip section. The nonlinear acoustic parameter in the grip section for all samples is very close to each other and it is about 5. On the other hand, near the fracture section it varies between 14 and 17. A large increase of 320% is observed as the fracture edge is approached. The curves are nearly exponential for each of the samples. TEM was used to image the microstructure on a sample fatigued in similar LCF conditions and sections for TEM were taken at three different locations along the length on a fatigue fractured sample. It is observed in Fig. 6(a) that TEM images near the grip section show nearly dislocation free grain structure and the nonlinearity parameter is small. At an intermediate region, increase in dislocation density is observed, and nonlinear parameter in the same region has increased by about 30%. Images of the microstructure near the fracture edge show large increase in dislocation density as well as formation of entanglement. In this region, the nonlinearity parameter has increased by 320%. The dislocation density determined from the TEM images, taken at four different locations along the length of the sample is shown in Fig. 6(a). It is observed that as the dislocation density increases, the nonlinearity parameter also increases. Hence, a direct correlation is observed between dislocation density and nonlinearity parameter, as expected.

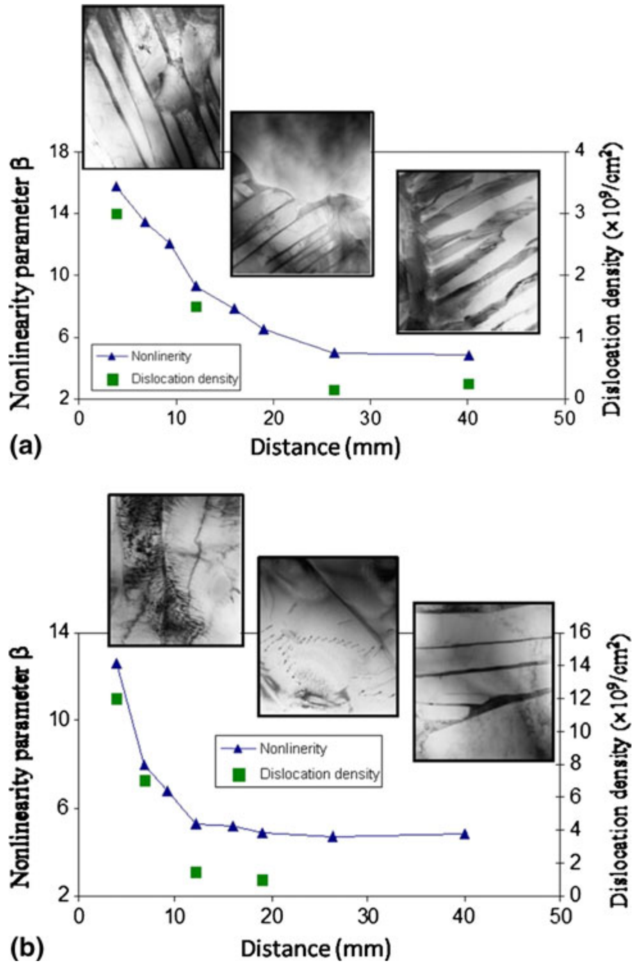

Fig. 6 Absolute nonlinearity parameter and dislocation density as a function of distance from the fracture surface for Ti-6Al-4V samples correlated with TEM observations. The specimens were fatigued under (a) low cycle fatigue (LCF) conditions and (b) high cycle fatigue (HCF) conditions

A sample fatigue-fractured under HCF condition of $\sigma_{max} = 620$ MPa, $R = 0.1$, $f = 10$ Hz was used for evaluating the local measurement of nonlinearity parameter under HCF conditions. The variation in nonlinear acoustic parameter along the length of the sample is shown in Fig. 6(b). The nonlinearity parameter exhibits an increase of 300%. The actual value of the parameter in the grip section is about 5 and closer to the fracture edge, it increases to about 13. The nonlinearity parameter remains at the same level as that of the grip section nearly 75% of the entire length of the sample. It dramatically increases to maximum in the remaining 25% of the length near the fracture region. A comparison of TEM microstructure with the variation in nonlinear acoustic parameter along the length of the sample is shown in the same Fig. 6(b). As in the case of LCF test, the dislocation density determined from the TEM images taken at four different locations along the length of the sample is shown with the nonlinearity parameter. It is observed that as the dislocation density increases, the nonlinearity parameter also increases. Thus, a direct correlation is observed between dislocation density and nonlinearity parameter as it has been established in theoretical models.

Measurement of nonlinear acoustic parameter of specimens fractured under LCF and HCF conditions show clear distinction in their behavior. The nonlinearity parameter is almost the same for both types of samples in the grip section. As the distance increases from the grip section to the fracture edge, the parameter increases almost exponentially. The rate at which this increase occurs for the LCF and HCF is different. In the HCF sample, the nonlinearity remains at the virgin material level for nearly 75% of the length. From then on it increases dramatically to a high value of 12. On the other hand, the parameter in the LCF specimen starts to increase just after the grip section. The steepness in the curve is much lower than the HCF specimen. This behavior can be qualitatively explained using the dislocation dynamics models. In the case of LCF, a load sufficiently large enough is applied. This load is enough to create local plastic deformation in the gage section. Since the strain is uniform in the gage section, the strain would create local plasticity in all the favorably oriented grains. As the number of cycles increase, the dislocation density is uniformly distributed. TEM as well as positron annihilation show that the dislocation density varies across the length of the specimen. From the theoretical model of Granato-Lucke (Ref 19), it is expected that as the dislocation density increases, the attenuation is expected to increase. In the case of HCF, the load is much smaller than the LCF. An increase in fatigue damage is related to an increase in nonlinearity parameter. Thus, in the case of LCF, the damage is distributed over the entire length of the gage section. In the HCF sample, the nonlinearity variation is observed very close to the fractured region and the damage is distributed over a small region. Although it is believed that LCF produces distributed damage and HCF gives rise to local damage, the nonlinear acoustic parameter provides an experimental confirmation of this fact. Therefore, the nonlinear acoustic behavior can be utilized to estimate the level of damage and the volumetric distribution of damage.

4. Conclusions

This article demonstrates the ability of advanced NDE methods, based on ultrasonic microscopy and nonlinear acoustics, for characterization of damage and life monitoring of aging aerospace materials.

An innovative ultrasonic microscopy technique has been developed and successfully used for local elastic property measurement, crack size determination as well as to evaluate interfacial damage in high-temperature materials such as titanium matrix composites. The resolution of the technique depends on lens defocus from the surface of the sample. Depending on the defocus, ultrasonic microscopy can be used either to map the first layer of fibers or surface and subsurface features in the sample. The new technique was used to obtain Rayleigh velocity maps of the specimen through automated $V(z)$ curve acquisition and analysis using short-pulse ultrasound and overpasses the limitations of conventional SAW imaging. The choice of coupling medium was proved critical for using ultrasonic microscopy imaging of environmentally exposed specimens. Here, the capability of ultrasonic microscopy to determine crack sizes and evaluate interfacial damage was demonstrated.

Furthermore, the linear properties (velocity and attenuation) and nonlinear properties of Ti-6Al-4V material were continuously monitored during fatigue damage accumulation. Nonlinear properties have been measured. It is found that the material nonlinearity is very sensitive to fatigue mechanisms, much more than velocity and attenuation. The contribution of dislocations to the second harmonic and the overall material nonlinearity is confirmed by correlating nonlinear acoustic measurements with TEM imaging and determination of dislocation density. Three different regions of nonlinearity parameter behavior during the fatigue life have been identified, indicating different fatigue mechanisms. The first two regions show a slow increase followed by a quasi-linear increase then, after about 50% of life, saturation is reached until the final fracture. The same trend in the nonlinearity parameter during fatigue of different samples indicated "signature" behavior of acoustic nonlinearity during fatigue. Local evaluation of the nonlinearity parameter as a function of distance from the fracture section has been observed on Ti-6Al-4V samples fatigued under LCF and HCF conditions. An exponential increase in the nonlinearity parameter from the grip section to the fracture section has been observed, which is in correlation with dislocation density measurement.

References

1. D. Harmon and C. Saff, Metal Matrix Composites: Testing, Analysis, and Failure Modes, *Damage Initiation and Growth in Fiber Reinforced Metal Matrix Composites*, E.W.S. Johnson, Ed., ASTM STP 1032 (Philadelphia, PA), 1988, p 237–250
2. D.B. Marshall, B.N. Cox, and A.G. Evans, The Mechanics of Matrix Cracking in Brittle-Matrix Fiber Composites, *Acta Metall.*, 1985, **33**(11), p 2013–2021
3. L.N. McCartney, Mechanics of Matrix Cracking in Brittle-Matrix Fibre-Reinforced Composites, *Proc. R. Soc. Lond.*, 1987, **A409**, p 329–350
4. P. Karpur, T.E. Matikas, S. Krishnamurthy, and N. Ashbaugh, Ultrasound for Fiber Fragmentation Size Determination to Characterize Load Transfer Behavior of Matrix-Fiber Interface in Metal Matrix Composites, *Review of Progress in Quantitative NDE*, Vol 12B, D.O. Thompson and D.E. Chimenti, Ed., July 19-24, 1992 (La Jolla, CA), 1992, p 1507–1513
5. P. Karpur, T.E. Matikas, and S. Krishnamurthy, Matrix-Fiber Interface Characterization in Metal Matrix Composites Using Ultrasonic Imaging of Fiber Fragmentation, *Seventh Technical Conference on Composite Materials, Mechanics and Processing*, Vol 1, Amer. Soc. Composites, Pennsylvania State University (University Park, PA), 1992, p 420–427
6. T.E. Matikas and P. Karpur, Matrix-Fiber Interface Characterization in Metal Matrix Composites Using Ultrasonic Shear-Wave Back-Reflection Coefficient Technique, *Review of Progress in Quantitative NDE*, Vol 12B, D.O. Thompson and D.E. Chimenti, Ed., July 19-24, 1992 (La Jolla, CA), 1992, p 1515–1522
7. C.F. Quate, A. Atalar, and H.K. Wickramasinghe, Acoustic Microscopy with Mechanical Scanning—A Review, *Proc. IEEE*, 1979, **67**, p 1092–1114
8. R.A. Lemons and C.F. Quate, A Scanning Acoustic Microscope, *IEEE Ultrasonics Symposium*, Nov 5-7, 1973, p 18–21
9. G.A.D. Briggs, An Introduction to Scanning Acoustic Microscopy, *Microscopy Handbooks*, Oxford University Press-Royal Microscopical Society, Oxford, 1985, p 12
10. G.A.D. Briggs, *Acoustic Microscopy*, Oxford University Press, Oxford, 1992
11. C.W. Lawrence, G.A.D. Briggs, C.B. Scruby, and J.R.R. Davies, Acoustic Microscopy of Ceramic-Fibre Composites; Part I: Glass-Matrix Composites, *J. Mater. Sci.*, 1993, **28**, p 3635–3644
12. C.W. Lawrence, G.A.D. Briggs, and C.B. Scruby, Acoustic Microscopy of Ceramic-Fibre Composites; Part II: Glass–Ceramic-Matrix Composites, *J. Mater. Sci.*, 1993, **28**, p 3645–3652
13. C.W. Lawrence, G.A.D. Briggs, and C.B. Scruby, Acoustic Microscopy of Ceramic-Fibre Composites; Part III: Metal-Matrix Composites, *J. Mater. Sci.*, 1993, **28**, p 3653–3660
14. H.L. Bertoni, Rayleigh Waves in Scanning Acoustic Microscopy, *Rayleigh-Wave Theory and Application*, Vol 2, E.A. Ash and E.G.S. Paige, Ed., The Royal Institution, London, 1985, p 274–290
15. T.E. Matikas, M. Rousseau, and P. Gatignol, Theoretical Analysis for the Reflection of a Focused Ultrasonic Beam from a Fluid–Solid Interface, *J. Acoust. Soc. Am.*, 1993, **93**(3), p 1407–1416
16. K.K. Liang, G.S. Kino, and B.T. Khuri-Yakub, Material Characterization by the Inversion of V(z), *IEEE Trans. Sonics Ultrasonics*, 1985, **SU-32**(2), p 213–224
17. T.E. Matikas, Quantitative Short-Pulse Acoustic Microscopy and Application to Materials Characterization, *Microsc. Microanal.*, 2000, **6**, p 59–67
18. G. Lütjering, Property Optimisation Through Microstructural Control in Titanium and Aluminum Alloys, *Mater. Sci. Eng.*, 1999, **A263**, p 117–126
19. A. Granato and K. Lücke, Theory of Mechanical Damping due to Dislocations, *J. Appl. Phys.*, 1956, **27**, p 583

20. J.H. Cantrell and W.T. Yost, Acoustic Harmonic Generation from Fatigue-Induced Dislocation Dipoles, *Philos. Mag. A*, 1994, **69**(2), p 315–326
21. J. Frouin, S. Sathish, T.E. Matikas, and J.K. Na, Ultrasonic Linear and Nonlinear Behavior of Fatigued Ti-6Al-4V, *J. Mater. Res.*, 1998, **14**(4), p 1295–1298
22. J. Frouin, J. Maurer, S. Sathish, D. Eylon, J.K. Na, and T.E. Matikas, Real-Time Monitoring of Acoustic Linear and Nonlinear Behavior of Titanium Alloys During Cyclic Loading, *Nondestructive Methods for Materials Characterization*, Vol 591, Materials Research Society, 2000, p 79–84
23. J.E. Bailey and P.B. Hirsch, The Dislocation Distribution, Flow Stress and Stored Energy in Cold-Worked Polycrystalline Silver, *Philos. Mag.*, 1960, **5**, p 485–497
24. S.M. Allen, Foil Thickness Measurements from Convergent-Beam Diffraction Patterns, *Philos. Mag. A*, 1981, **43**, p 325–335
25. D.B. Williams and C.B. Carter, *Transmission Electron Microscopy: II. Diffraction*, Plenum Press, New York, 1996